MEDICAL ROBOTS

# Head-mounted surgical robots are an enabling technology for subretinal injections

**Nicholas R. Posselli[1,2], Eileen S. Hwang[3], Zachary J. Olson[1], Aaron Nagiel[4,5], Paul S. Bernstein[3], Jake J. Abbott[1]***



**Therapeutic protocols involving subretinal injection, which hold the promise of saving or restoring sight, are challenging for surgeons because they are at the limits of human motor and perceptual abilities. Excessive or insufficient indentation of the injection cannula into the retina or motion of the cannula with respect to the retina can result in retinal trauma or incorrect placement of the therapeutic product. Robotic assistance can potentially enable the surgeon to more precisely position the injection cannula and maintain its position for a prolonged period of time. However, head motion is common among patients undergoing eye surgery, complicating subretinal injections, yet it is often not considered in the evaluation of robotic assistance. No prior study has both included head motion during an evaluation of robotic assistance and demonstrated a significant improvement in the ability to perform subretinal injections compared with the manual approach. In a hybrid ex vivo and in situ study in which an enucleated eye was mounted on a human volunteer, we demonstrate that head-mounting a high-precision teleoperated surgical robot to passively reduce undesirable relative motion between the robot and the eye results in a bleb-formation success rate on moving eyes that is significantly higher than the manual success rates reported in the literature even on stationary enucleated eyes.**

## INTRODUCTION

Many up-and-coming therapeutic protocols in ophthalmology are challenging for surgeons to perform because they are near or beyond the limits of human motor and perceptual abilities. For example, the intended delivery method for the US Food and Drug Administration (FDA)–approved and European Medicines Agency (EMA)–approved gene therapy Luxturna, which treats patients with inherited retinal disease due to mutations in the *retinoid isomerohydrolase RPE65* (*RPE65*) gene, is via transvitreal subretinal injection (*1*). In transvitreal subretinal injections, the surgeon performs a vitrectomy, introduces an injection cannula into the eye through the pars plana, gently places the cannula in contact with the retinal surface, and then attempts to inject a prespecified volume of the therapeutic product into the subretinal space between the photoreceptors and the retinal pigment epithelium (RPE). The injected liquid causes the retina to locally separate from the RPE; the separated retina with subretinally injected liquid is known as a bleb. Positioning the cannula to avoid retinal trauma and to achieve repeatability in injection dosage (i.e., volume of injected product) is challenging. The retina is approximately 300 μm thick (*2*), and the peak-to-peak magnitude and root mean square amplitude of hand tremors in retinal surgeons have been reported to be 108 μm (*3*) and 156 μm (*4*), respectively. In addition, microjerks of approximately 250 μm have been observed during manual static positioning (*5*).

Subretinal injections can be complicated by motion of the eye. Patients receive a nerve block to induce paralysis of the eye in its orbit, but that does not reduce motion of the orbit itself. Conscious sedation, which is often used for eye surgery (*6*), makes patients calm and drowsy but leaves them still able to breathe and respond to their environment. Head motion, and thus orbit motion, in this state is due to breathing, talking, swallowing, snoring [which affects 16% of patients (*7*)], and other voluntary and involuntary patient motions. Magnitudes of relative displacements between a surgical instrument and the retina due to patient head motion, which are on the order of several millimeters (*8*), greatly exceed the magnitudes that are due to hand tremor. Movement must be compensated by the surgeon, to the best of their ability, to avoid complications, but sudden movements can be unpredictable. Currently, patients receiving gene therapy are often placed under general anesthesia (*9*). General anesthesia reduces motion of the patient, but it has its own associated risks (*10*). Because of such risks, conscious sedation is typically preferred for other types of retinal surgery.

Motion of the injection cannula relative to the retina during injection, whether it is due to unintended motion of the surgeon's hand or the patient's head, can result in retinal trauma such as retinal tears (*11*) or enlargement of the retinotomy through which the therapeutic product is injected, which may increase reflux of the product into the vitreous cavity. Reflux of the therapeutic product can lead to inflammation (*12*) and a discrepancy between the intended volume and the actual volume that makes it into the subretinal space. Hsu *et al.* (*13*) conducted a study in which the volume of liquid injected into the subretinal space was, on average, only 39.6% of the target volume, and the surgeon always underestimated the amount of leakage.

The limited depth perception offered by microscopic visualization of the retina makes it difficult to determine when the cannula is at an ideal depth to raise the subretinal bleb. Insufficient indentation or penetration of the cannula into the retina can lead to injection into the vitreous cavity, intraretinal hydration, or retinoschisis (*14*, *15*), whereas excessive indentation can cause hemorrhage, damage to the RPE, or injection of the product into the sub-RPE space (*14*, *15*). Given the difficulties in estimating the depth of the cannula, one clinical approach to forming a bleb is to start injecting the product before the cannula is in contact with the retina. The

[1]Robotics Center and Department of Mechanical Engineering, University of Utah, Salt Lake City, UT 84112, USA. [2]Department of Biomechanical Engineering, University of Twente, 7522 NB Enschede, Netherlands. [3]Moran Eye Center, Department of Ophthalmology and Visual Sciences, University of Utah, Salt Lake City, UT 84132, USA. [4]Roski Eye Institute, Department of Ophthalmology, Keck School of Medicine, University of Southern California, Los Angeles, CA 90033, USA. [5]Vision Center, Department of Surgery, Children's Hospital Los Angeles, Los Angeles, CA 90027, USA.
*Corresponding author. Email: jake.abbott@utah.edu

surgeon then moves the cannula closer to the retina until they visually identify the initiation of a bleb. However, this results in wastage of the therapeutic product into the vitreous cavity, with the associated aforementioned problems. Intraoperative optical coherence tomography (OCT) provides a cross-sectional view of the retina alongside the en face microscope image so that the surgeon can estimate the insertion depth of the cannula. However, it can still be difficult for the surgeon to assimilate the visual information from the OCT and the microscope (*14*), and they must do so while simultaneously keeping the cannula steady with respect to a moving eye.

Recent studies suggest that slowing the flow rate of the injected product, which is determined by the injection pressure (*16*), may be safer (*16*–*20*) and result in more consistent bleb volumes (*5*, *17*). To evaluate the effect of flow rate on the RPE and surrounding tissue, Scruggs *et al.* (*19*) compared a "fast" flow rate of 1.8 ml/min and a "slow" flow rate of 0.18 ml/min against eyes in which there was no injection and found that there was a significant difference in RPE gene expression between the 1.8 ml/min case and the no-injection case, but they found no significant difference between the 0.18 ml/min case and the no-injection case. Takahashi *et al.* (*16*) evaluated the effect of injection pressure on retinal damage in monkeys and found that retinal damage increased with injection pressure; they concluded that subretinal injection pressure should be as low as possible to minimize damage. Scruggs *et al.* (*20*) conducted an in-human study in which patients received gene therapy and found that low injection pressures were associated with prolonged injection durations and that there are minimum pressures that must be exceeded for initiating and propagating the bleb. Ladha *et al.* (*5*) identified reflux from the retinotomy when the cannula was removed after bleb formation; they stated that the reflux was due to tension within the bleb and that such reflux would be reduced by prolonging the cannula's placement in the subretinal space. It has been suggested that maintaining the cannula's position in the subretinal space for as long as 15 to 20 min may even be desirable (*17*).

A variety of robotic systems have been proposed to improve retinal surgery (*21*, *22*), including subretinal injection. Here, we focus on the transvitreal route for subretinal injections, which is the most popular, although other routes are also possible (*23*). Robotic assistance may enable the surgeon to keep the cannula positioned in the subretinal space for a prolonged period of time, which would enable injections to be performed using lower flow rates. Robotic assistance may also reduce the attention necessary by the surgeon to maintain the cannula's position so that they can alternate their attention between the en face view from the microscope and the cross-sectional OCT images to better estimate the depth of the cannula. Some valuable contributions have been made toward achieving more repeatable subretinal injections, including methods to estimate the insertion depth of the injection cannula (*24*–*27*) and to automate the placement of the cannula at a desired depth in the retina (*28*–*31*).

However, any robotic system will have to contend with the aforementioned movement of the eye. Several research groups have reported results for robot-assisted subretinal injections in stationary ex vivo eyes (*31*–*37*) or stationary artificial eyes (*31*, *38*). Some of these groups achieved high success rates, but it is unclear what success rate they would have achieved if head motions were considered. Only the in vivo study with the PRECEYES Surgical System has captured the effect of patient motion during subretinal injection (*17*), noting that preliminary results from this study were described in (*39*). That study compared the number of retinotomies, volume of liquid injected, duration of liquid delivery, total duration of surgery, number of microtrauma events (i.e., inadvertent retinal touches and retinal microhemorrhages), and postoperative visual acuity between the robot-assisted and manual approaches. Although their results were encouraging, they stated that they did not observe superiority of robotic assistance over their manual results. Further, they described difficulties initiating subretinal injection in one patient because of head drift.

A variety of methods have been proposed to passively reduce unintended relative motion between the surgical instrument and the retina, with the goal of achieving the superhuman precision promised by robotic assistance. The current standard in robot-assisted retinal surgery is strapping down the patient's head on the stretcher pillow (*17*), which is effective at reducing gross head drift but is not particularly effective at reducing within-breathing-cycle motion. In (*40*), we found that within-breathing-cycle displacements of the eye orbit relative to a stationary frame were estimated to be ~2 mm during gentle breathing and 5 mm during snoring-like movements, even with the head strapped down. Beyond simply strapping down the patient's head on the stretcher pillow, there are three main approaches: immobilize the patient's head (*41*–*43*), immobilize the patient's eye (*17*, *39*, *43*, *44*), or mount the surgical robot(s) to the patient's head (*40*, *45*, *46*). Attempting to noninvasively immobilize (the surface of) the patient's head can still allow movement of the patient's body to translate into movement of the eye, orbit, and retina due to the compliance of the soft tissue surrounding the skull. Attempting to noninvasively immobilize (the anterior of) the patient's eye can still result in retinal movement due to the soft-tissue compliance of the eye. Noninvasively mounting surgical robots rigidly to the skull, via the upper jaw (*45*), seems impractical unless the surgical robot(s) could be made very light. For these reasons, we have chosen to pursue mounting surgical robot(s) to the head via mask or helmet-type devices that are custom-fit to the contours of the patient's head (*40*). The hypothesized benefit is that, by not attempting to immobilize the patient's head or eye, the forces that cause soft-tissue deformation would tend to remain small. We recently measured an order-of-magnitude reduction in within-breathing-cycle relative motion compared with a pillow rest with a head strap while also eliminating gross relative motion (*40*); it is noteworthy that the device does not reduce motion of the head itself. Although the reduction in relative motion demonstrated the potential for the head-mounting concept to improve surgical performance, the robot used in (*40*) was not active, nor was it used to perform any actual surgical tasks.

In this study, we used one of the two head-mounting design concepts presented in (*40*) to demonstrate that a head-mounted high-precision surgical robot is an enabling technology for consistently initiating subretinal injections and propagating the resulting blebs using slow injection flow rates, even in the presence of head motion. We modified the surgical robot from (*47*), which is one of the smallest, lightest, and most precise retinal-surgery robots developed to date (*21*, *22*); hardware modifications enabled the use of a clinical cannula and improved the kinematic conditioning for the transvitreal route, and software modifications implemented virtual fixtures for assisting the user during teleoperation and enabled the actuation of the clinical cannula. We also modified our goggles from (*48*) that enable an enucleated eye to be mounted directly in front of the eye of a healthy human volunteer, which results in a new type of hybrid ex vivo and in situ study in which we are able to capture motion and

soft-tissue effects of a living human head, which is critical to the evaluation of our head-mounting device, while performing surgical procedures on animal tissues.

## RESULTS

### Experimental setup for the hybrid ex vivo and in situ study

Figure 1 shows the experimental setup of this study. We used the head-mounting device described in (*40*) that is a modification of a commercial radiotherapy immobilization system to noninvasively mount a modified version of the robot described in (*47*) to a volunteer's head. The head-mounting device was used to reduce the relative motion between the robot and the head. The lightweight (0.8 kg) robot uses piezoelectric stick-slip actuators and has an instrument-positioning precision of better than 1 μm (*47*). The robot hardware was modified to enable the attachment and actuation of an extendable subretinal-injection cannula. We mounted an open-sky (i.e., with the anterior portion removed; details on the preparation of the eyes are provided in Materials and Methods) ex vivo porcine eye to the volunteer's head using a modified version of the eye-mounting goggles introduced in (*48*), which enables patient head motion to be simulated given that the orbit of the mounted eye moves with the orbit of the volunteer's eye. The eye-mounting goggles also allow the mounted eye to rotate because of forces and moments exerted on scleral trocar cannulas by surgical instruments, with a rotational stiffness matching that of an anesthetized patient's eye (*48*). The robot was teleoperated using a Phantom Omni haptic device (not shown) to bring the tip of the subretinal injection cannula into contact with the retina, and a custom syringe pump was used to inject saline at a constant flow rate into the subretinal space. A pressure sensor was used to record injection pressure at the outlet of the syringe. A Heidelberg Spectralis OCT system provided an en face view of the retina using infrared (IR) reflection imaging and a cross-sectional view of the retina using OCT, which enabled us to verify the placement of the cannula before starting to inject, verify that the fluid was injected into the subretinal space, and observe the size of the bleb (movie S1).

The head-mounting device used in this study was previously described in (*40*). It uses a custom-fit thermoplastic mask and internal cushion, which were formed to the shape of the volunteer's head before the experiment. During the experiment, the head-mounting device rested on the pillow of an eye-surgery stretcher (HillRom, Chicago, IL, USA) while the volunteer lay supine. Because only one robot was attached to the head-mounting device, counterweights were placed on the opposite side to avoid a moment being felt by the volunteer. The weights of the robot and counterweights were distributed around the rigid device and carried by the stretcher pillow, rather than being carried by the patient. Most of the soft-tissue deformation between the patient's skull and the device occurred when the patient first rested their head on the stretcher pillow, before the surgical procedure started; subsequent soft-tissue deformation during the procedure due to breathing, etc., was small compared with the initial deformation.

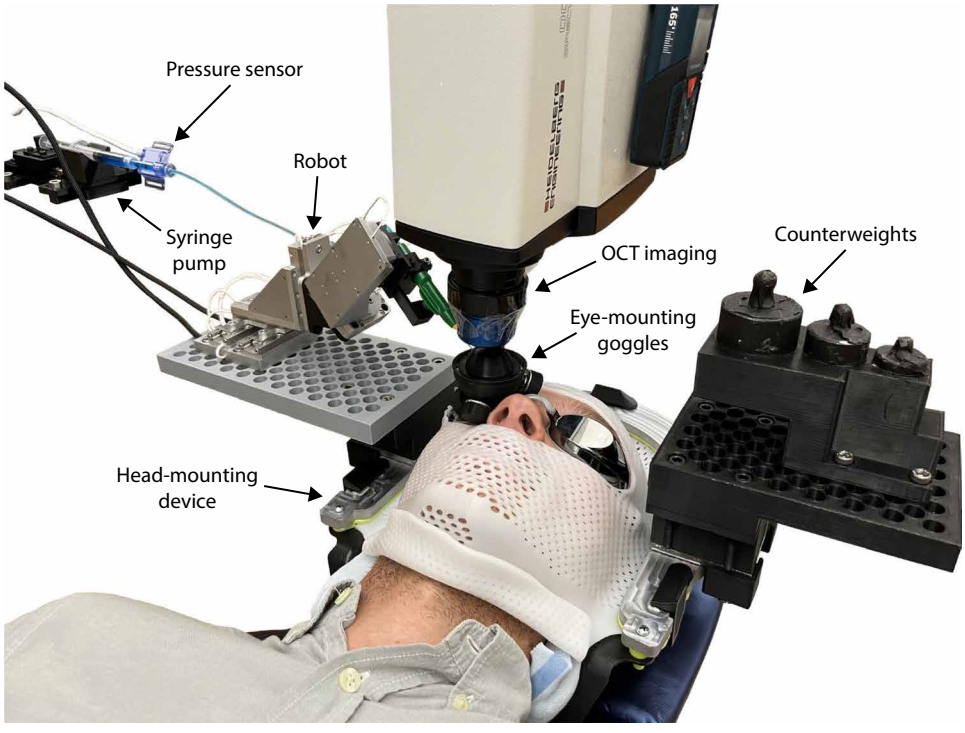


**Fig. 1. Apparatus for the subretinal-injection experiment.** Subretinal injections were performed in ex vivo eyes using a teleoperated robot mounted to the head of a volunteer who was lying supine on an eye-surgery stretcher. The head-mounting device passively reduced relative motion between the robot and the volunteer's head. The eye-mounting goggles, which held an ex vivo porcine eye, coupled the motion of the porcine eye to the orbit of the volunteer's eye to enable head and eye motion to be taken into account without endangering the volunteer's eye. OCT imaging was used to visualize the placement of the injection cannula relative to the retina. The table that the syringe pump rests on, and other background elements in the image, have been removed for clarity.

### Modifications to the robot hardware

We modified the robot described in (*47*) to improve the kinematic conditioning of the robot for transvitreal subretinal injections under OCT and to enable the attachment and actuation of an extendable subretinal-injection cannula (Fig. 2). For our experiments, which were in open-sky ex vivo porcine eyes, optimal imaging quality was achieved when the OCT system was positioned only a few centimeters above the eye. To avoid collision between the robot and the OCT system, and to prevent the robot from obstructing the OCT image, the robot should hold the instrument such that its angle from the horizontal plane is approximately 45° or less. However, for the original robot in (*47*) (Fig. 2A), the robot was farthest from its wrist singularity when the instrument was held vertically. To improve the kinematic conditioning of the robot, we introduced a 45° angled component (Fig. 2B).

The instrument holder of the robot described in (*47*) was replaced to enable the use of a 25-gauge/38-gauge (25-g/38-g) extendable PolyTip subretinal-injection cannula (MedOne Surgical, Sarasota, FL,

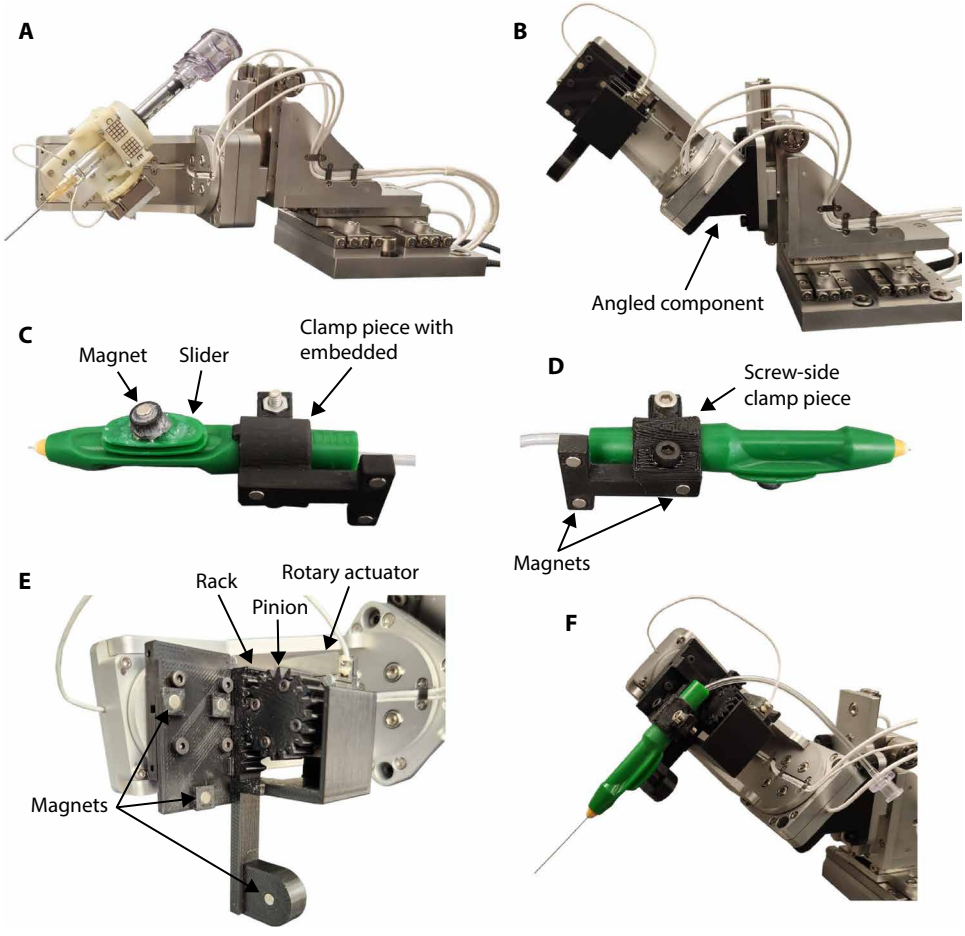


**Fig. 2. Modifications made to the robot to enable subretinal injections.** (**A**) Original robot described in (*47*). (**B**) 45° angled component to improve the kinematic conditioning for the transvitreal route. (**C**) Magnet attachment for extendable-cannula slider and the component of the magnetic instrument-holder clamp that has embedded magnets. (**D**) Component of the magnetic instrument holder that clamps the instrument in place by screwing into the magnet-embedded clamp piece. (**E**) 3D-printed components for magnetic attachment of subretinal-injection cannula. A rack-and-pinion mechanism enables the robot's rotary actuator to actuate the extendable-cannula slider. (**F**) Fully assembled modified robot.

USA) (Fig. 2C). A 3D-printed instrument-mounting plate with embedded magnets was attached to the second-most distal rotary joint of the robot. We repurposed the most distal rotary actuator in (*47*), which previously rotated the instrument about its long axis, to convert its rotary motion to linear motion using a rack-and-pinion mechanism; given the symmetry of the blunt-tip cannula used in this work, rotation about the axis of the cannula was unnecessary. A 3D-printed component connected the repurposed actuator to the instrument-mounting plate, and a 3D-printed pinion was mounted directly to the repurposed actuator. The pinion meshed with a 3D-printed rack that slid along a guiding slot in the mounting plate. A 3D-printed cover was placed over the pinion to prevent future sterile draping from getting pinched in the mechanism. The cover also contained a guiding slot to constrain the rack such that it remained within the guide slot of the mounting plate. We created a two-part instrument holder using 3D-printed components that, when screwed together, clamped onto the handle of the subretinal-injection cannula (Fig. 2, C and D). Magnets embedded in the instrument holder attached to the magnetic mounting plate on the robot. A 3D-printed component with an embedded magnet was glued to the cannula's slider, which extended or retracted the inner 38-g cannula, using a cyanoacrylate adhesive so that the magnet in the rack magnetically connected to the slider. The forces and/or torques required to displace or detach the instrument were higher than those that occurred during retinal surgery, but the instrument could easily be manually removed from the robot when desired. We note that many of the auxiliary components described above could be eliminated if they were simply manufactured into future single-use commercial devices.

### Modifications to the eye-mounting goggles

The eye-mounting goggles, introduced in (*48*), were used to mount an ex vivo porcine eye to the volunteer's head so that the orbit of the mounted eye moved with the orbit of the volunteer's eye. Because we chose to remove the anterior section of each ex vivo eye, the surgical instrument could not pass through a scleral trocar cannula as it would in an actual surgery. However, in an actual surgery, forces between the surgical instrument and the scleral trocar cannula result in movement of the eye and thus movement of the retina. To maintain this behavior, we modified the eye-mounting goggles to include an artificial anterior section of the eye (Fig. 3), which enabled us to insert a trocar cannula into the artificial sclera. A rigid 3D-printed component simulating the anterior sclera was attached to the top of the bowl of the eye-mounting goggles using double-sided tape. To simulate the compliance at the scleral trocar cannula due to the soft tissue of the sclera, we cut out a patch of the rubber sclera component of a commercial eye phantom (Phake-i Surgical Training System, Hilco Vision, Mansfield, MA, USA) and glued it over a hole in the 3D-printed artificial sclera. We then inserted a 25-g trocar cannula into the rubber patch.

### OCT imaging

A Heidelberg Spectralis OCT system (Heidelberg Engineering, Franklin, MA, USA; Fig. 1) provided simultaneous IR reflection imaging and OCT images that were used to view the cannula and retina (Fig. 4). Similar to an operating microscope, the IR reflection imaging provided an en face view of the retina and cannula. However, unlike operating microscopes, the IR reflection images were monoscopic, so they did not provide depth information. OCT provides a cross-sectional visualization (i.e., B-scan) of the retina and cannula, which enabled us to estimate the depth of the cannula with respect to the retina. The OCT system was suspended above the volunteer's head

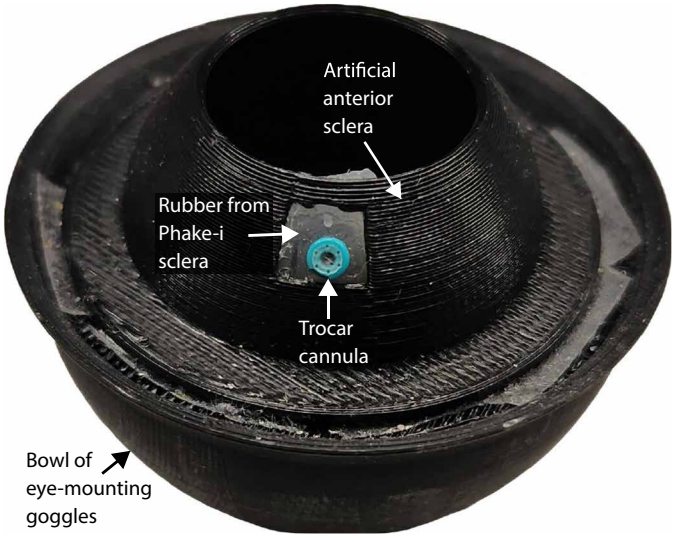


**Fig. 3. Modified eye-mounting goggles.** An artificial anterior sclera, with an embedded trocar cannula, was attached to the bowl component of the eye-mounting goggles. This modification enabled the open-sky eyes used in our experiment to rotate because of forces and moments applied by the instrument on the trocar cannula.

using a heavy-duty mounting arm attached to a cart. The cart was placed superior to the volunteer, who lay supine on the stretcher. Because we removed the cornea and lens of each eye, thus changing the optics, we attached a mouse lens (Heidelberg Engineering) to the OCT system, which resulted in higher-quality OCT scans. After the instrument was aligned with the trocar cannula, but before the instrument was moved to the center of the eye, the OCT system's focus knob and the distance between the OCT system and the eye were adjusted to achieve clear IR reflection and OCT images. When imaging the insertion depth of the cannula, the location of the B-scan plane was manually set in the Heidelberg Eye Explorer software by dragging the scan line in the IR reflection image to the location of the cannula's tip, and the scan plane was continually adjusted as the eye moved under the OCT system because of head motion.

## Teleoperation

The robot was teleoperated using a Phantom Omni haptic device placed on the OCT cart. The haptic device was oriented in a comfortable position for the operator of the robot, and then the spatial transformation between the robot and haptic-device coordinate frames was adjusted in software such that displacements of the haptic device stylus caused the instrument to move in an intuitive direction. The OCT was oriented such that the mapping of the surgical instrument's motion to the IR reflection image on the computer monitor matched the mapping that is familiar to a retinal surgeon looking into the eyepieces of an operating microscope.

To insert the instrument into the eye, the backdrivable nature of the robot's piezoelectric stick-slip actuators enabled the robot to be manually positioned such that the tip of the instrument coincided with the trocar cannula; the location of the instrument's tip in the base coordinate frame of the robot was then saved in the software and used as the remote center of motion (RCM).

Motion of the robot was enabled when one of the two buttons on the haptic-device stylus was depressed and held and was otherwise disabled. If the user wanted to release the haptic-device stylus or recenter the stylus in the haptic device's workspace, then they disabled the motion of the robot by releasing the motion-enabling button. Whenever the motion-enabling button was depressed, the position of the instrument was indexed to the position of the haptic device; this prevented the instrument from moving suddenly when robot motion was enabled.

A one-degree-of-freedom (one-DOF) virtual fixture automatically constrained the motion of the robot to insertion or retraction motions along the axis of the instrument until the tip of the instrument was near the center of the eye, at which point the robot entered a teleoperation mode in which the scaled position of the haptic device was mapped to the position of the instrument's tip (i.e., the tip of the 25-g metal cannula) while enforcing the RCM constraint. While within this teleoperation mode, the user could depress both buttons on the haptic-device stylus to engage a one-DOF virtual fixture that constrained the tip of the instrument to move vertically while still implementing the RCM constraint; this virtual fixture was used whenever the cannula compressed the retina. The 38-g polymer cannula was extended or retracted by the user by interacting with the graphical user interface. Additional details about the teleoperation of the robot are provided in Materials and Methods.

## Experiment to measure the success rate of bleb formation

We conducted an experiment to measure the success rate of bleb formation using the head-mounted robot. We recruited one volunteer, who was instructed to lie still and breathe normally. A member of the engineering team teleoperated the robot after he had sufficient practice performing the procedure. For each attempt to initiate a bleb, the pump dispensed 0.3 ml [which is the intended injection volume for Luxturna (*1*)] of saline at a constant flow rate of 0.18 ml/min, which is the "slow" flow rate described by Scruggs *et al.* (*19*). We considered each injection a success if a bleb formed at the initial injection site. We chose this metric for success to exclude scenarios in which the injection failed to form a bleb at an initial location on the retina but succeeded after moving the cannula to a subsequent location, because such a scenario risks retinal trauma at multiple locations.

For the 21 bleb-formation attempts, we made one attempt in the first eye and then two attempts in each of the subsequent 10 eyes with the injection sites selected on opposite halves of the retina. Each injection site was selected to avoid injecting next to the optic nerve, near the edge of the retina, or directly into a visible blood vessel. For each attempt, we teleoperated the robot using a motion-scaling factor of 80 to move the injection cannula toward the middle of the retina until its tip was visible in the IR reflection image, after which point the user interacted with the robot's graphical user interface to fully extend the 38-g cannula. The cannula was then moved toward the retina until it was ~300 μm above the retina, at which point the motion-scaling factor was set to 150 and the virtual fixture that constrains the cannula tip to move vertically was activated. On the basis of the findings of (*14*), which showed that partial indentation of the retina was associated with failure to create a bleb, we positioned the cannula such that it fully compressed the retina (Fig. 4), after which point we started the syringe pump. It took 100 s for the pump to dispense 0.3 ml of saline at a flow rate of 0.18 ml/min. If after 20 s a bleb had not started to form, the operator made small vertical adjustments at their discretion, using a vertical virtual fixture, to attempt to initiate a bleb. After the pump stopped, we waited for the measured pressure to drop below 0.5 psi, at which point we

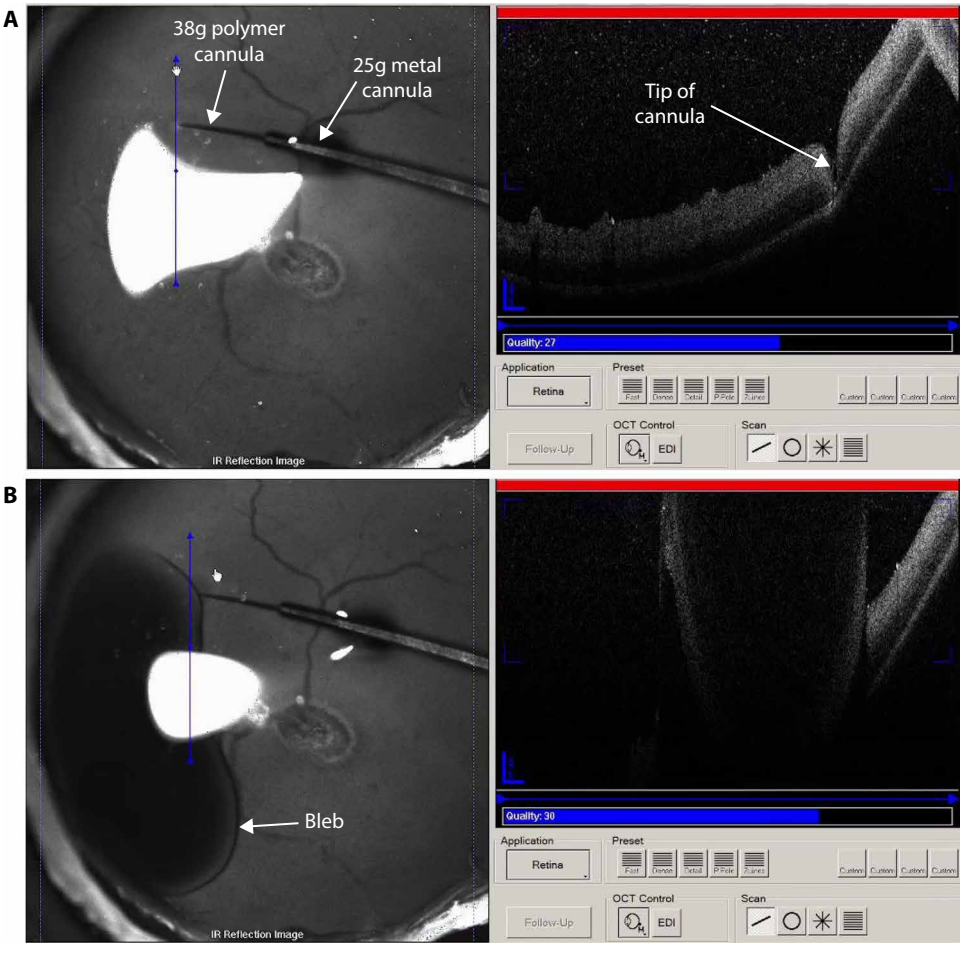


**Fig. 4. IR reflection (left) and OCT (right) images taken during a subretinal injection.** (**A**) The cannula fully indented the retina immediately before starting the syringe pump. (**B**) Bleb initiation and expansion is visible under IR reflection and OCT imaging. The OCT penetration depth was insufficient to capture the full height of the fully formed bleb. The outline of the bleb in the OCT image appears to be upside down because of a mirror artifact. Note that the bright areas in the IR reflection images are simply reflections.

retracted the 38-g inner cannula, moved the cannula away from the retina, and removed the instrument from the eye.

## Bleb-formation success rate

We successfully initiated bleb formation in 100% of the $n = 21$ attempts, which gives a 95% confidence interval on the true success rate of (84.5 to 100%) (Fig. 5). We combined available results in the literature for manual injection results in stationary ex vivo eyes (*33*, *34*, *36*) for a total reported success rate of 63.6% with $n = 44$, from which we calculated a 95% confidence interval on the true success rate of (48.9 to 76.2%). The individual available studies have reported success rates and calculated 95% confidence intervals as follows: Yang *et al.* (*34*) reported 100% success with $n = 5$, for a 95% confidence interval of (56.6 to 100%); Maierhofer *et al.* (*36*) reported 61.8% success with $n = 34$, for a 95% confidence interval of (45.0 to 76.1%); and Ladha *et al.* (*33*) reported 40% success with $n = 5$, for a 95% confidence interval of (11.8 to 76.9%). Our bleb-formation results represent a significant difference ($P < 0.001$) compared with the combined results for surgeons' manual injections in stationary ex vivo eyes (*33*, *34*, *36*). Our findings also represent a significant difference compared with two of the three individual studies in that group [i.e., (*33*) and (*36*)]. Although no difference was found with the remaining study in that group [i.e., (*34*)], which had 100% success with $n = 5$, their 95% confidence interval indicates that the true success rate may be much lower, consistent with the estimate from the combined results.

During two of our injection attempts, the bleb did not form within 20 s of the pump starting (an arbitrary time that we established for ourselves, before which we would not make any intervention), so we made slight (≤100 μm) vertical adjustments to the cannula; we did not have to move the cannula to a different location on the retina and cause additional retinal trauma. In one of the attempts, the bleb began to form after an adjustment downward, and in the other attempt, the bleb formed after an adjustment upward then downward; the difference was simply due to our desire to explore different strategies. In these two cases, the slow injection rate gave sufficient time to correct for suboptimal cannula placement such that the bleb could begin to form before even 25% of the volume was dispensed, and a high-precision robot combined with a virtual fixture that constrained the cannula tip to move vertically enabled the necessary adjustments to be made in a controlled fashion. Surgeons make slight vertical adjustments during manual injections, whether intentionally or unintentionally, and the position of the needle during injection has been shown to be unsteady (*36*). As a result, we classified our two injection attempts with slight vertical corrections as successes, particularly for the comparison with the manual results of surgeons reported in the literature.

However, it is also potentially interesting to reconsider our results using a more stringent standard in which we classify the need to make any corrections as a failure; this standard is only applicable to robotic systems. Using this more stringent definition of success, we successfully initiated bleb formation in 90.5% of the $n = 21$ attempts, which gives a 95% confidence interval on the true success rate of (71.1 to 97.3%).

## Additional observations and measurements

Head-mounting greatly reduces, but does not fully eliminate, unintended relative motion between the instrument and the eye (*40*). We found that the compliance in the 38-g polymer cannula passively compensated for the remaining relative motion, such that the tip of the cannula seemed to stay fixed with respect to the indented retina.

We measured injection pressures of ~5 psi (table S1). Although it was not our primary metric of success, we were also interested in whether the cannula was sufficiently positioned to propagate

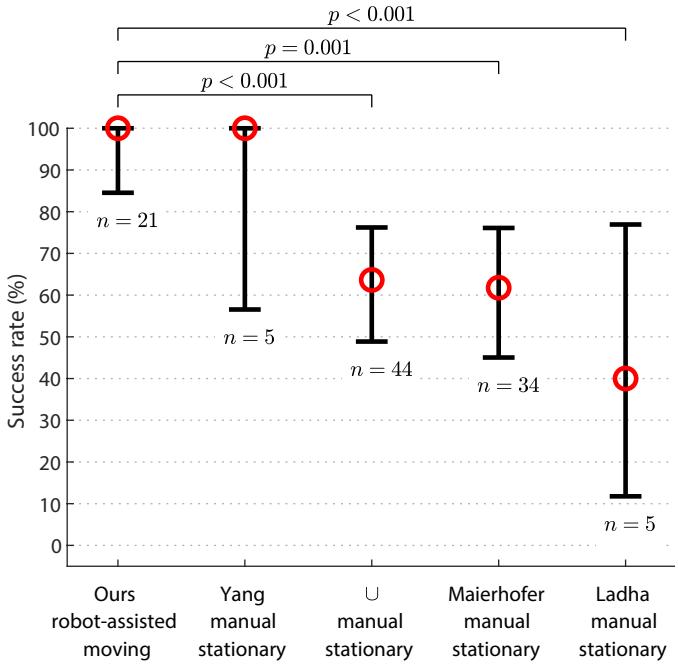


**Fig. 5. Comparisons of bleb-formation success rates.** We made comparisons of the success rate of our head-mounted robot on moving enucleated eyes with the surgeons' manual bleb-formation success rate on stationary enucleated eyes from Yang *et al.* (*34*), Maierhofer *et al.* (*36*), and Ladha *et al.* (*33*), as well as the combined results (i.e., union ∪) from those three studies. For each dataset, we denote the experimental success rate (red circle) and the 95% confidence interval that was calculated using the Wilson score interval on the true success rate (see Materials and Methods). *P* values, which were calculated using Barnard's test (see Materials and Methods), are provided for each hypothesis test for which there exists a difference between experimental results.

the bleb throughout the slow injections. We measured the duration of bleb expansion for 17 of the injections (fig. S4): 10 blebs expanded for at least the full 100 s, 5 expanded for 90 s, 1 expanded for 70 s, and 1 expanded until the cannula was intentionally lifted at 20 s.

## DISCUSSION

Our results indicate that head-mounting a low-mass, high-precision, teleoperated surgical robot enables one to achieve a high success rate forming subretinal blebs, despite the natural motions typical of patients undergoing eye surgery. We compared our results with those reported in the literature for surgeons forming blebs in stationary eyes, and we would expect results for surgeons treating moving ex vivo eyes (results that do not exist in the literature) to be worse, given that it is self-evident that a manual injection in a moving eye is more difficult than a manual injection in a stationary eye. However, the difference in the degree of difficulty is poorly understood. During manual surgery, the surgeon will often rest their hands directly on the patient's head, which serves to reduce their hand tremor and couple the motion of their hands with the patient's head, similar to the coupling accomplished by head-mounting a robot; this suggests that differences between manual injections in vivo and ex vivo might not be as substantial as one might think.

A clinical workflow describing how a robot can be magnetically connected to the head-mounting device through sterile draping placed over the patient is presented in (*40*). It is possible for small robots such as ours to be sterilized via gas or autoclave; the manufacturer of our robot's actuators (SmarAct GmbH) makes autoclavable versions. In addition, the magnetic cannula attachment could enable sterile draping to be placed over the robot before the attachment of the cannula. We created a custom after-market magnetic-attachment component for a commercial cannula, but in the future, such components could be integrated into the commercial devices directly.

It should be noted that there are differences in the tissue-preparation methods between groups conducting subretinal-injection experiments. For example, some groups have used whole eyes with regulated intraocular pressure. The pressure on the retinas of the open-sky eyes used in our experiments would be lower, which could decrease the injection pressure required to raise a bleb. However, it is not clear whether this would make it any easier to successfully raise a bleb, particularly considering how easy it was with our system to make slight vertical adjustments to ensure a good seal between the cannula and the retina.

There are also differences in the surgical techniques between groups. Some groups described puncturing through the retina (*17*, *33*, *34*, *36*, *37*), and groups used either metal- (*36*) or polymer-tipped (*17*, *35*) cannulas that could be beveled or unbeveled. We used a cannula with an unbeveled polymer tip to indent, but not puncture, the retina. It is possible that these choices contributed to our success rate. It is worth noting that the effect of the cannula and surgical technique is confounded with the effect of the robotic system in all prior studies of robot-assisted subretinal injection.

The state-of-the-art solution for intraoperative imaging during subretinal injection is intraoperative OCT, which supplements stereoscopic operating-microscope images with OCT images. However, we did not have access to such a system that could be used with animal tissues. Our ability to achieve a high success rate using an OCT system that only provides a monocular en face view may be further evidence of the benefits afforded by head-mounting.

If desired, further reduction in relative motion between the cannula and the retina can likely be achieved if head-mounting is used in conjunction with other compensation methods, such as immobilizing the eye relative to the robot (*17*, *39*, *43*, *44*) or using active feedback control (*49*–*53*); because head-mounting substantially reduces relative motion between the robot and the head (*40*), head-mounting would make it easier to compensate for any remaining relative motion using these other methods. These other methods may also be necessary for cases in which there is residual eye movement due to an incomplete paralysis from the nerve block (*54*).

## MATERIALS AND METHODS

### Study design

The overall objective of the study was to test the hypothesis that the robot-assisted bleb-formation success rate on moving ex vivo eyes is better than the manual bleb-formation success rate of surgeons on stationary ex vivo eyes (which would be as good as, if not better than, the manual bleb-formation success rate of surgeons on moving ex vivo eyes). Bleb formation was determined by visual inspection of IR-reflection images and OCT images. A given bleb

formation was determined as a success if it was formed at the initial location selected on the retina.

In pilot testing, we had been obtaining a 100% success rate using the robotic system. As such, we assumed that we would obtain at least a 95% success rate in the study, so to find a significant difference from the combined results from the literature for manual injections in stationary ex vivo eyes, it would require at least $n = 20$ eyes if we were to use a significance of $\alpha = 0.01$. On any given day of testing, we would use all of the enucleated eyes that we had obtained from the abattoir until we reached or surpassed this number. If we were to obtain a success rate less than 95%, we could repower the study at that time; this was not necessary. All attempts at bleb formation were included in the calculation of the success rate (i.e., there were no exclusion criteria). In the end, we stopped the study after $n = 21$ eyes.

### Ethics approval for human-participant research

Under the approval of the University of Utah Institutional Review Board, the experiment comprised one healthy 25-year-old adult male volunteer (see Fig. 1). Informed consent was obtained after the nature and possible consequences of the study were explained.

### Preparation of ex vivo eyes

Fresh ex vivo porcine eyes were obtained from a local butcher on each day of experimentation. The eyes were kept on ice and used between 2 and 8 hours postmortem. We removed the tissues surrounding the eye (e.g., fatty tissues, muscles, and optic nerve) and then used cyanoacrylate adhesive to adhere the posterior surface of the eye to a 3D-printed bowl insert (i.e., a thin-walled bowl). We created a variety of bowl inserts of different inner diameters to accommodate different eye sizes but with outer diameters that matched the inner diameter of the bowl component of our eye-mounting goggles. During pilot testing, we found that removing the vitreous, which is typical of retinal surgery, made it easier to raise a bleb. To remove the vitreous without the use of a vitrectomy console and permit imaging despite postmortem clouding of the cornea and lens, we removed the anterior section of the eye by cutting the sclera circumferentially 3 to 5 mm below the limbus. The vitreous typically remained attached to the anterior section of the eye and could be lifted from the retina. Care was taken to avoid detaching the retina. If substantial retinal detachments were observed, then the eye was discarded. Immediately after removing the vitreous, the posterior portion of the eye was filled with physiological saline. We then placed the bowl insert holding the eye into the bowl of the eye-mounting goggles; double-sided tape was used to ensure that the bowl insert did not rotate within the bowl of the eye-mounting goggles.

### Injection methods

The custom syringe pump comprised 3D-printed components attached to a Thorlabs MTS50/M motorized translation stage (Thorlabs, Newton, NJ, USA) (Fig. 1 and fig. S1). The 3D-printed components hold the barrel of a 3-ml syringe in place on the stationary base of the motorized stage and attach the syringe plunger to the stage's moving platform. We used Thorlabs APT software to program the motion of the motorized stage. The velocity $v$ (units mm/s) of the stage was calculated on the basis of the desired flow rate $Q = 3$ µl/s [i.e., $Q = 0.18$ ml/min, which is the "slow" flow rate from (*19*)] and the inner area of the syringe barrel, $A = 63.6\,\text{mm}^2$: $v = Q/A = 47.2$ µm/s. To displace a volume of $V = 0.3$ ml of liquid from the syringe, which is the intended injection volume for Luxturna (*1*), the stage was moved by a distance $d = V/A = 4.7$ mm. After the stage's motion is initiated, it moves for 100 s.

A PRESS-S-000 pressure sensor (PendoTech, West Windsor Township, NJ, USA) was attached directly to the outlet of the syringe. After the syringe pump finished depressing the syringe plunger, there was still pressure built up in the injection tubing. Lifting the cannula away from the retina while there is still built-up pressure may result in leakage from the cannula, but the pressure sensor enabled us to wait until the pressure dropped below 0.5 psi, after which point we retracted the inner cannula and removed the instrument from the eye.

### Additional teleoperation details

The low-level position controller of the robot was the same as the one described in (*47*), except we used $k_f = 1$ for the constant associated with the frequency at which the actuators' step displacements should be commanded. Similar to (*47*), when pivoting the instrument about the RCM, a singularity occurred when the tip of the instrument coincided with the RCM, so the instrument was automatically constrained to insertion or retraction motions along the axis of the instrument when the tip of the instrument was within 10 mm of the trocar cannula, using a one-DOF virtual fixture. When the cannula was inside of the eye and more than 10 mm away from the trocar cannula, the robot automatically entered the teleoperation mode in which the scaled position of the haptic device was mapped to the position of the instrument's tip (i.e., the tip of the 25-g metal cannula) while enforcing the RCM constraint.

Unlike in (*47*), in which the user could control four DOFs of the instrument's pose (i.e., three-DOF Cartesian position of the instrument's tip and rotation of the instrument about its long axis), only the three-DOF Cartesian position of the instrument's tip could be controlled in our study because of the repurposing of one rotary actuator to move the slider on the extendable subretinal-injection cannula; for the symmetric blunt-tip cannula used in this work, rotation about the axis of the cannula was unnecessary.

To extend or retract the 38-g polymer cannula, the user entered a desired distance for extension or retraction in a text box in the graphical user interface. The extension or retraction occurred when the user pressed a button in the user interface. The actuator used to actuate the cannula's slider did not have a sensor, so the distance of extension or retraction was an estimate based on prior measurements of the actuator's step size. The amount of extension or retraction was iteratively adjusted by the user on the basis of the amount of extension observed in the IR reflection image.

### Statistical analysis

The Wilson score interval was used to calculate confidence intervals on success rates. It is an improvement to the conventional method of calculating confidence intervals, particularly in cases with a small number of trials or with extreme success or failure rates. The Wilson score interval is calculated as

$$\left(\frac{\hat{p}+\frac{z^2}{2n}}{1+\frac{z^2}{n}}\right)\pm\left(\frac{z}{1+\frac{z^2}{n}}\right)\sqrt{\frac{\hat{p}(1-\hat{p})}{n}+\frac{z^2}{4n^2}} \quad (1)$$

where $\hat{p} \in [0, 1]$ is the experimental success rate expressed as a proportion of $n$ trials, and the $z$ value used is dependent on the

confidence interval of interest (e.g., a 95% confidence interval uses $z = 1.96$). Note that the resulting confidence interval, which is also expressed in terms of proportions, is not centered on $\hat{p}$.

To calculate the $p$ value for a given hypothesis test, we formed a two-way contingency table containing the number of successes and failures of each group being compared and used Barnard's test. Barnard's test is an exact test that can be used for small samples, but it is also valid for larger sample sizes. We used the implementation of Barnard's test provided by the Exact package for the R programming language (*55*). In each call to the Exact package's exact.test function, the optional function arguments were passed in as follows: alternative = "two.sided," npNumbers = 1000, method = "csm," model = "Binomial," and tsmethod = "square."

## Supplementary Materials

**The PDF file includes:**
Methods
Figs. S1 to S4
Table S1
Legend for movie S1

**Other Supplementary Material for this manuscript includes the following:**
Movie S1
MDAR Reproducibility Checklist

## REFERENCES AND NOTES


1. Luxturna [package insert] (Spark Therapeutics, Inc., 2022).
2. C. E. Myers, B. E. Klein, S. M. Meuer, M. K. Swift, C. S. Chandler, Y. Huang, S. Gangaputra, J. W. Pak, R. P. Danis, R. Klein, Retinal thickness measured by spectral-domain optical coherence tomography in eyes without retinal abnormalities: The Beaver Dam Eye Study. *Am. J. Ophthalmol.* **159**, 445–456.e1 (2015).
3. S. P. N. Singh, C. N. Riviere, Physiological tremor amplitude during retinal microsurgery, in *Proceedings of the IEEE 28th Annual Northeast Bioengineering Conference* (IEEE, 2002), pp. 171–172.
4. F. Peral-Gutierrez, A. L. Liao, C. N. Riviere, Static and dynamic accuracy of vitreoretinal surgeons, in *Proceedings of the 26th Annual International Conference of the IEEE Engineering in Medicine and Biology Society* (IEEE, 2004), pp. 2734–2737.
5. R. Ladha, L. E. Caspers, F. Willermain, M. D. de Smet, Subretinal therapy: Technological solutions to surgical and immunological challenges. *Front. Med.* **9**, 846782 (2022).
6. J. F. Salmon, B. Mets, M. F. James, A. D. Murray, Intravenous sedation for ocular surgery under local anaesthesia. *Br. J. Ophthalmol.* **76**, 598–601 (1992).
7. C. A. McCannel, E. J. Olson, M. J. Donaldson, S. J. Bakri, J. S. Pulido, M. Donna, Snoring is associated with unexpected patient head movement during monitored anesthesia care vitreoretinal surgery. *Retina* **32**, 1324–1327 (2012).
8. K. Brogan, B. Dawar, D. Lockington, K. Ramaesh, Intraoperative head drift and eye movement: Two under addressed challenges during cataract surgery. *Eye* **32**, 1111–1116 (2018).
9. J. Gao, R. M. Hussain, C. Y. Weng, Voretigene neparvovec in retinal diseases: A review of the current clinical evidence. *Clin. Ophthalmol.* **14**, 3855–3869 (2020).
10. A. A. Sallam, P. H. Donachie, T. H. Williamson, J. M. Sparrow, R. L. Johnston, The Royal College of Ophthalmologists' National Ophthalmology Database study of vitreoretinal surgery: Report 5, anaesthetic techniques. *Br. J. Ophthalmol.* **100**, 246–252 (2016).
11. S. Russell, J. Bennett, J. A. Wellman, D. C. Chung, Z.-F. Yu, A. Tillman, J. Wittes, J. Pappas, O. Elci, S. McCague, D. Cross, K. A. Marshall, J. Walshire, T. L. Kehoe, H. Reichert, M. Davis, L. Raffini, L. A. George, F. P. Hudson, L. Dingfield, X. Zhu, J. A. Haller, E. H. Sohn, V. B. Mahajan, W. Pfeifer, M. Weckmann, C. Johnson, D. Gewaily, A. Drack, E. Stone, K. Wachtel, F. Simonelli, B. P. Leroy, J. F. Wright, K. A. High, A. M. Maguire, Efficacy and safety of voretigene neparvovec (AAV2-hRPE65v2) in patients with RPE65-mediated inherited retinal dystrophy: A randomised, controlled, open-label, phase 3 trial. *Lancet* **390**, 849–860 (2017).
12. F. F. Reichel, F. Wozar, I. Seitz, A. Ochakovski, K. U. Bartz-Schmidt, T. Peters, M. D. Fischer, RD-CURE Consortium, An optimized treatment protocol for subretinal injections limits intravitreal vector distribution. *Ophthalmol. Sci.* **1**, 100050 (2021).
13. S. T. Hsu, H. Gabr, C. Viehland, K. Sleiman, H. T. Ngo, O. M. Carrasco-Zevallos, L. Vajzovic, R. P. McNabb, S. S. Stinnett, J. A. Izatt, A. N. Kuo, C. A. Toth, Volumetric measurement of subretinal blebs using microscope-integrated optical coherence tomography. *Transl. Vis. Sci. Technol.* **7**, 19 (2018).
14. H. M. Vasconcelos Jr., B. J. Lujan, M. E. Pennesi, P. Yang, A. K. Lauer, Intraoperative optical coherence tomographic findings in patients undergoing subretinal gene therapy surgery. *Int. J. Retina Vitr.* **6**, 13 (2020).
15. C. Irigoyen, A. Amenabar Alonso, J. Sanchez-Molina, M. Rodríguez-Hidalgo, A. Lara-López, J. Ruiz-Ederra, Subretinal injection techniques for retinal disease: A review. *J. Clin. Med.* **11**, 4717 (2022).
16. K. Takahashi, Y. Morizane, T. Hisatomi, T. Tachibana, S. Kimura, M. M. Hosokawa, Y. Shiode, M. Hirano, S. Doi, S. Toshima, R. Araki, H. Matsumae, Y. Kanzaki, M. Hosogi, A. Yoshida, K.-H. Sonoda, F. Shiraga, The influence of subretinal injection pressure on the microstructure of the monkey retina. *PLOS ONE* **13**, e0209996 (2018).
17. J. Cehajic-Kapetanovic, K. Xue, T. L. Edwards, T. C. Meenink, M. J. Beelen, G. J. Naus, M. D. de Smet, R. E. MacLaren, First-in-human robot-assisted subretinal drug delivery under local anesthesia. *Am. J. Ophthalmol.* **237**, 104–113 (2022).
18. K. Xue, M. Groppe, A. Salvetti, R. MacLaren, Technique of retinal gene therapy: Delivery of viral vector into the subretinal space. *Eye* **31**, 1308–1316 (2017).
19. B. A. Scruggs, C. Jiao, C. M. Cranston, E. Kaalberg, K. Wang, S. R. Russell, L. A. Wiley, R. F. Mullins, E. M. Stone, B. A. Tucker, E. H. Sohn, Optimizing donor cellular dissociation and subretinal injection parameters for stem cell-based treatments. *Stem Cells Transl. Med.* **8**, 797–809 (2019).
20. B. A. Scruggs, H. M. Vasconcelos Jr., M. Matioli da Palma, K. Kogachi, M. E. Pennesi, P. Yang, S. T. Bailey, A. K. Lauer, Injection pressure levels for creating blebs during subretinal gene therapy. *Gene Ther.* **29**, 601–607 (2022).
21. E. Vander Poorten, C. N. Riviere, J. J. Abbott, C. Bergeles, M. A. Nasseri, J. U. Kang, R. Sznitman, K. Faridpooya, I. Iordachita, *Handbook of Robotic and Image-Guided Surgery*, M. H. Abedin-Nasab, Ed. (Elsevier, 2019), chap. 36, pp. 627–672.
22. I. I. Iordachita, M. D. De Smet, G. Naus, M. Mitsuishi, C. N. Riviere, Robotic assistance for intraocular microsurgery: Challenges and perspectives. *Proc. IEEE* **110**, 893–908 (2022).
23. E. Z. Ahronovich, N. Shihora, J.-H. Shen, K. Joos, N. Simaan, Exploring an external approach to subretinal drug delivery via robot assistance and B-mode OCT, in *2023 IEEE International Conference on Robotics and Automation (ICRA)* (IEEE, 2023), pp. 6795–6801.
24. M. Zhou, Q. Yu, K. Huang, S. Mahov, A. Eslami, M. Maier, C. P. Lohmann, N. Navab, D. Zapp, A. Knoll, M. A. Nasseri, Towards robotic-assisted subretinal injection: A hybrid parallel–serial robot system design and preliminary evaluation. *IEEE Trans Ind Electron* **67**, 6617–6628 (2020).
25. M. Sommersperger, J. Weiss, M. A. Nasseri, P. Gehlbach, I. Iordachita, N. Navab, Real-time tool to layer distance estimation for robotic subretinal injection using intraoperative 4D OCT. *Biomed. Opt. Express* **12**, 1085–1104 (2021).
26. S. Wei, J. W. Kim, A. Martin-Gomez, P. Zhang, I. Iordachita, J. U. Kang, Region targeted robotic needle guidance using a camera-integrated optical coherence tomography, in *Biophotonics Congress: Biomedical Optics 2022 (Translational, Microscopy, OCT, OTS, BRAIN)*, (Optica Publishing Group, 2022), p. CM2E.6.
27. M. Zhou, X. Guo, M. Grimm, E. Lochner, Z. Jiang, A. Eslami, J. Ye, N. Navab, A. Knoll, M. A. Nasseri, Needle detection and localisation for robot-assisted subretinal injection using deep learning. *CAAI Trans. Intell. Technol.*, 10.1049/cit2.12242 (2023).
28. G. W. Cheon, Y. Huang, J. Cha, P. L. Gehlbach, J. U. Kang, Accurate real-time depth control for CP-SSOCT distal sensor based handheld microsurgery tools. *Biomed. Opt. Express* **6**, 1942–1953 (2015).
29. J. Im, C. Song, Oblique injection depth correction by a two parallel OCT sensor guided handheld SMART injector. *Biomed. Opt. Express* **12**, 926–939 (2021).
30. S. Lee, J. U. Kang, CNN-based CP-OCT sensor integrated with a subretinal injector for retinal boundary tracking and injection guidance. *J. Biomed. Opt.* **26**, 068001 (2021).
31. P. Zhang, J. W. Kim, P. Gehlbach, I. Iordachita, M. Kobilarov, Autonomous needle navigation in subretinal injections via iOCT. *IEEE Robot. Autom. Lett.* **9**, 4154–4161 (2024).
32. J. U. Kang, G. W. Cheon, Demonstration of subretinal injection using common-path swept source OCT guided microinjector. *Appl. Sci.* **8**, 1287 (2018).
33. R. Ladha, J. Smit, T. Meenink, L. E. Caspers, F. Willermain, M. D. De Smet, Defining parameters for robotic or manual reflux-free subretinal injections in an ex vivo animal model. *Investig. Ophthalmol. Vis. Sci.* **61**, 4485 (2020).
34. K. Yang, X. Jin, Z. Wang, Y. Fang, Z. Li, Z. Yang, J. Cong, Y. Yang, Y. Huang, L. Wang, Robot-assisted subretinal injection system: Development and preliminary verification. *BMC Ophthalmol.* **22**, 484 (2022).
35. A. Abid, R. Duval, C. Boutopoulos, Development and ex-vivo validation of 36g polyimide cannulas integrating a guiding miniaturized OCT probe for robotic assisted subretinal injections. *Biomed. Opt. Express* **13**, 850–861 (2022).
36. N. A. Maierhofer, A.-M. Jablonka, H. Roodaki, M. A. Nasseri, A. Eslami, J. Klaas, C. P. Lohmann, M. Maier, D. Zapp, iOCT-guided simulated subretinal injections: A comparison between manual and robot-assisted techniques in an ex-vivo porcine model. *J. Robot. Surg.* **17**, 2735–2742 (2023).
37. H. Roodaki, N. A. Maierhofer, A.-M. Jablonka, A. Nasseri, C. P. Lohmann, A. Eslami, OCT-based volumetric measurement of subretinal injection blebs in ex-vivo porcine eyes. *Investig. Ophthalmol. Vis. Sci.* **61**, 472 (2020).

38. R. Ladha, T. Meenink, J. Smit, M. D. de Smet, Advantages of robotic assistance over a manual approach in simulated subretinal injections and its relevance for gene therapy. *Gene Ther.* **30**, 264–270 (2023).
39. T. L. Edwards, K. Xue, H. C. M. Meenink, M. J. Beelen, G. J. L. Naus, M. P. Simunovic, M. Latasiewicz, A. D. Farmery, M. D. de Smet, R. E. MacLaren, First-in-human study of the safety and viability of intraocular robotic surgery. *Nat. Biomed. Eng.* **2**, 649–656 (2018).
40. N. R. Posselli, P. S. Wellborn, P. S. Bernstein, R. J. Webster III, J. J. Abbott, Head-mounting surgical robots for passive compensation of patient motion. *J. Med. Robot. Res.* **9**, 2350006 (2024).
41. M. A. Nasseri, M. Eder, S. Nair, E. C. Dean, M. Maier, D. Zapp, C. P. Lohmann, A. Knoll, The introduction of a new robot for assistance in ophthalmic surgery, in *Annual International Conference of the IEEE Engineering in Medicine and Biology Society* (IEEE, 2013), pp. 5682–5685.
42. K. Huang, M. Zhou, C. Lajblich, C. P. Lohmann, A. Knoll, Y. Ling, H. Lin, M. A. Nasseri, A flexible head fixation for ophthalmic microsurgery, in *2017 Chinese Automation Congress (CAC)* (IEEE, 2017), pp. 6707–6710.
43. M. A. Nasseri, M. Maier, C. P. Lohmann, A targeted drug delivery platform for assisting retinal surgeons for treating age-related macular degeneration (AMD), in *Annual International Conference of the IEEE Engineering in Medicine and Biology Society* (IEEE, 2017), pp. 4333–4338.
44. S. Guo, N. R. Sarfaraz, W. G. Gensheimer, A. Krieger, J. U. Kang, Demonstration of optical coherence tomography guided big bubble technique for deep anterior lamellar keratoplasty (DALK). *Sensors* **20**, 428 (2020).
45. W. Wei, R. Goldman, N. Simaan, H. Fine, S. Chang, Design and theoretical evaluation of micro-surgical manipulators for orbital manipulation and intraocular dexterity, in *Proceedings 2007 IEEE International Conference on Robotics and Automation* (IEEE, 2007), pp. 3389–3395.
46. W. Wei, R. E. Goldman, H. F. Fine, S. Chang, N. Simaan, Performance evaluation for multi-arm manipulation of hollow suspended organs. *IEEE Trans. Robot.* **25**, 147–157 (2008).
47. M. Nambi, P. S. Bernstein, J. J. Abbott, A compact telemanipulated retinal-surgery system that uses commercially available instruments with a quick-change adapter. *J. Med. Robot. Res.* **1**, 1630001 (2016).
48. N. R. Posselli, P. S. Bernstein, J. J. Abbott, Eye-mounting goggles to bridge the gap between benchtop experiments and in vivo robotic eye surgery. *Sci. Rep.* **13**, 15503 (2023).
49. B. C. Becker, R. A. MacLachlan, L. A. Lobes, G. D. Hager, C. N. Riviere, Vision-based control of a handheld surgical micromanipulator with virtual fixtures. *IEEE Trans. Robot.* **29**, 674–683 (2013).
50. A. Ebrahimi, M. G. Urias, N. Patel, R. H. Taylor, P. Gehlbach, I. Iordachita, Adaptive control improves sclera force safety in robot-assisted eye surgery: A clinical study. *IEEE Trans. Biomed. Eng.* **68**, 3356–3365 (2021).
51. Y. Han, A. Routray, J. O. Adeghate, R. A. MacLachlan, J. N. Martel, C. N. Riviere, Monocular vision-based retinal membrane peeling with a handheld robot. *J. Med. Devices* **15**, 031014 (2021).
52. X. He, J. Handa, P. Gehlbach, R. Taylor, I. Iordachita, A submillimetric 3-DOF force sensing instrument with integrated fiber Bragg grating for retinal microsurgery. *IEEE Trans. Biomed. Eng.* **61**, 522–534 (2014).
53. H. Natalius, P. Lambert, M. K. Tiwari, L. da Cruz, C. Bergeles, "Design, Static and Performance Analysis of a Parallel Robot for Head Stabilisation in Vitreoretinal Surgery" in *New Trends in Medical and Service Robotics. MESROB 2020. Mechanisms and Machine Science*, G. Rauter, P. C. Cattin, A. Zam, R. Riener, G. Carbone, D. Pisla, Eds. (Springer, 2021), vol. 93, pp. 169–179.
54. D. Roman-Pognuz, G. Scarpa, G. Virgili, E. Roman-Pognuz, G. Paluzzano, F. Cavarzeran, Comparison of retrobulbar, sub-tenon anesthesia and medial canthus episcleral anesthesia for 25-gauge posterior vitrectomy. *Retina* **42**, 19–26 (2022).
55. P. Calhoun, Exact: Unconditional exact test, R package version 3.2. (2022); https://doi.org/10.32614/cran.package.exact.


**Acknowledgments:** We thank L. McCoy, J. Allen, B. Korous, B. Jones, and S. Becker from the Moran Eye Center at the University of Utah for lending equipment and providing technical assistance. We also thank Circle V Meat for the donations of the eyes used in this study. **Funding:** This study was supported in part by the National Eye Institute (NEI) of the National Institutes of Health (NIH) grants R21EY027528 (J.J.A. and P.S.B.), K08EY034549 (E.S.H.), P30 EY014800 (E.S.H. and P.S.B.), and K08EY030924 (A.N.); in part by an unrestricted grant to the Department of Ophthalmology and Visual Sciences at the University of Utah from Research to Prevent Blindness (E.S.H. and P.S.B.); in part by an unrestricted grant to the Department of Ophthalmology at the University of Southern California (USC) Keck School of Medicine from Research to Prevent Blindness (A.N.); in part by the Las Madrinas Endowment in Experimental Therapeutics for Ophthalmology (A.N.); in part by a Research to Prevent Blindness Career Development Award (A.N.); and in part by a Knights Templar Eye Foundation Endowment (A.N.). **Author contributions:** J.J.A., P.S.B., E.S.H., and A.N. conceptualized the research and acquired the funding. N.R.P., E.S.H., Z.J.O., A.N., J.J.A., and P.S.B. developed the methodology for the study. J.J.A. and E.S.H. provided resources. N.R.P. and Z.J.O. gathered the experimental data. N.R.P. curated the data and developed the software and visualizations. N.R.P. and J.J.A. performed the statistical analysis of the data. N.R.P., J.J.A., E.S.H., A.N., and P.S.B. wrote and edited the manuscript. **Competing interests:** A.N. is a consultant for Eyebiotech, Ultragenyx, Blackstone, Immuneering, Lexitas, Astellas, and Janssen. All other authors declare that they have no competing interests. **Data and materials availability:** All data needed to evaluate the conclusions in the paper are present in the paper or the Supplementary Materials. Supplementary data and code supporting the findings of this study are publicly available on Dryad at the following link: https://doi.org/10.5061/dryad.w0vt4b91w.

Submitted 10 April 2024
Accepted 22 January 2025
Published 19 February 2025
10.1126/scirobotics.adp7700

Science Robotics

# Head-mounted surgical robots are an enabling technology for subretinal injections

Nicholas R. Posselli, Eileen S. Hwang, Zachary J. Olson, Aaron Nagiel, Paul S. Bernstein, and Jake J. Abbott

*Sci. Robot.* **10** (99), eadp7700. DOI: 10.1126/scirobotics.adp7700







*Science Robotics* (ISSN 2470-9476) is published by the American Association for the Advancement of Science. 1200 New York Avenue NW, Washington, DC 20005. The title *Science Robotics* is a registered trademark of AAAS.